Bipolar Monte Carlo Simulation of Hot Carriers in III-N LEDs

Pyry Kivisaari*, Toufik Sadi†, Jingrui Li‡, Vihar Georgiev†, Jani Oksanen§, Patrick Rinke‡ and Jukka Tulkki§
*Division of Solid State Physics, Lund University, Lund, Sweden. Email: pyry.kivisaari@ftf.lth.se
†Device Modeling Group, School of Engineering, University of Glasgow, Glasgow, UK
‡Department of Applied Physics, Aalto University, Aalto, Finland
§Department of Neuroscience and Biomedical Engineering, Aalto University, Aalto, Finland

***Abstract*—We carry out bipolar Monte Carlo (MC) simulations of electron and hole transport in a multi-quantum well light-emitting diode with an electron-blocking layer. The MC simulation accounts for the most important interband recombination and intraband scattering processes and solves self-consistently for the non-quasiequilibrium transport. The fully bipolar MC simulator results in better convergence than our previous Monte Carlo–drift-diffusion (MCDD) model and also shows clear signatures of hot holes. Accounting for both hot electron and hot hole effects increases the total current and decreases the efficiency especially at high bias voltages. We also present our in-house full band structure calculations for GaN to be coupled later with the MC simulation in order to enable even more detailed predictions of device operation.**

I. Introduction

Light-emitting diodes (LEDs) based on III-Nitrides are revolutionizing the field of general lighting with their very high efficiency and improving spectral tunability [1]. However, in spite of superior performance as compared to competing lighting technologies, the III-N LEDs of today still suffer from a decrease in the efficiency at high input powers (aka efficiency droop). In spite of roughly ten years of intensive research of the efficiency droop, complete understanding of its origins is still missing [2]. In addition to the efficiency droop, the device-level understanding of III-N multi-quantum well (MQW) LEDs on a more general level remains incomplete. The most obvious example of this is that the commonly used device simulation models typically result in notably higher bias voltages than observed experimentally. To remedy these problems, more research is needed in developing device simulation models that account more accurately for microscopic processes taking place in LEDs.

Most of the device models used for III-N LEDs today are based on the drift-diffusion (DD) model, in which electrons and holes are modeled by quasi-equilibrium distributions [3], [4]. The DD model is very useful in interpreting the device-level characteristics of LEDs but is inherently based on quasi-equilibrium carrier distributions. However, recent measurements indicate that the carrier distributions in III-N LEDs exhibit some hot-carrier properties already in typical operating conditions [5], [6]. In order to generate more insight to these measurements, we recently developed a Monte Carlo-drift-diffusion (MCDD) model, which accounts for the physics of hot electrons in the simulation of LEDs. According to MCDD simulations, Auger recombination generates population of hot electrons, part of which is even expected to reach the p-type contact [7], [8]. At large bias voltages the MCDD and DD results also differ from each other, suggesting a breakdown of the DD model [9].

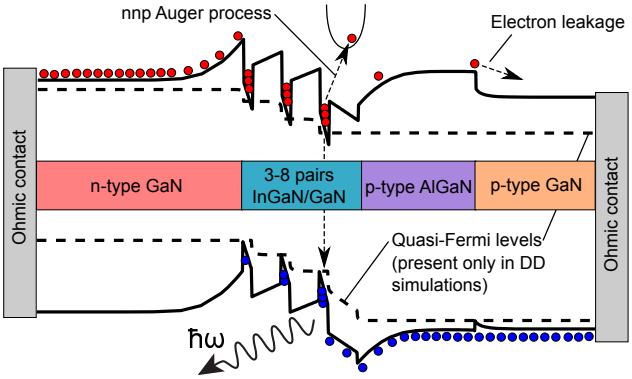

Fig. 1. Schematic figure of the III-N LEDs studied in this work. The figure also illustrates radiative recombination, an *nnp* Auger process, and a regular electron leakage process.

In this paper we carry out fully bipolar Monte Carlo (MC) simulations, in which both electrons and holes are simulated using MC, taking into account all the relevant scattering and recombination processes and device physics. The simulations are performed for the III-N LED device illustrated in Fig. 1. In this paper we especially study how the full bipolar MC simulation affects hole transport. For faster convergence, initial values are taken from a standard DD simulations. We also present full band structure calculations to be used later in more detailed device simulations. All the important intraband scattering processes are directly included in MC simulations. The MC simulations also account for the recombination processes, which are calculated using the carrier densities from the MC simulation.

II. Theory

To model the effects of non-quasiequilibrium charge transport on device characteristics, one no longer can rely on the DD model and assume that the electron and hole populations are in internal equilibrium. To account for the full energy spectrum of electrons and holes, in this paper we therefore use MC models to simulate electron and hole transport throughout the whole device for a given bias voltage. Hot-carrier effects resulting from Auger recombination, high electric fields, and

978-1-4673-7860-4/15/$31.00 ©2015 IEEE

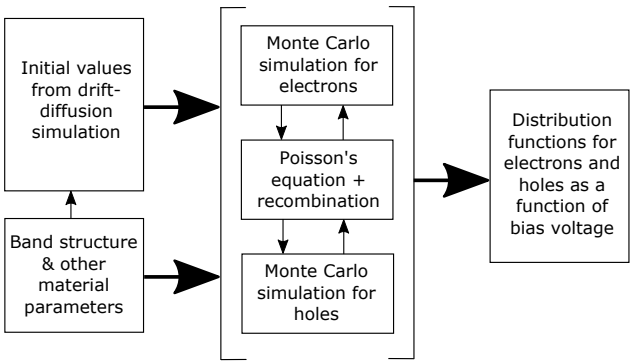

Fig. 2. Diagram of the full bipolar MC simulation. Initial values for the electron and hole distributions as well as the band diagram are taken from a DD simulation. The MC simulations run together with Poisson's equation and recombination rates provide the distribution functions of electrons and holes throughout the full device as a function of bias voltage.

large band offsets are thereby included directly, and carrier relaxation within the bands is modeled through the various intraband scattering processes.

Figure 2 shows the diagram of the full bipolar MC simulation method. To provide initial values for the MC simulation for faster convergence, a DD simulation is first performed for the whole device. Electron and hole densities, band diagrams and recombination rates are taken from the DD simulation and used as a starting point in the MC simulation. The MC simulation is run for both electrons and holes, and electron and hole densities are used to update the electric fields and recombination rates during the simulation. After the band edges and recombination rates have converged, the simulation is continued to collect final results for the distribution functions as time averages from the full MC simulation.

A. Hot carrier transport

To fully account for hot-carrier effects, the standard MC model is employed to solve the Boltzmann's transport equation (BTE). More specifically, the transport of carriers is modeled by simulating their equations of motion during free flights, and by using random numbers to generate scattering events based on specific scattering rates. To enable generating free-flight times from a homogeneous Poisson-distribution, self-scattering is used to model a virtual scattering event in which the wavevector of the carrier does not change. Application of MC models specifically in III-N LEDs is discussed in our earlier works [7]–[10], and more details of the MC simulation model itself can be found in Refs. [11]–[15].

B. Intraband scattering

Intraband scattering processes change the electronic states of carriers within the conduction or the valence band. Each separate scattering process *m* has a scattering rate $W_m(\mathbf{k}, \mathbf{k}')$, given the carriers initial and final states $\mathbf{k}$ and $\mathbf{k}'$, respectively. For constructing the scattering ladder and generating free-flight times, the rates are integrated over all the possible $\mathbf{k}'$ to provide $W_m(\mathbf{k})$. The simulations of this paper include deformation potential acoustic and optical phonon scattering, polar optical phonon scattering, piezoelectric acoustic phonon scattering, ionized impurity scattering due to ionized dopant atoms, carrier-carrier scattering, alloy disorder scattering, and surface roughness scattering at material interfaces. Detailed expressions for calculating the scattering rates are provided, e.g., in references [11], [16], [17].

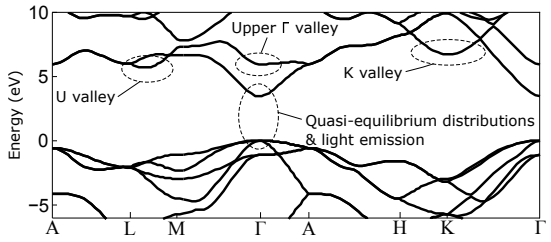

Fig. 3. Band structure of GaN calculated with the HSE hybrid functional. The figure also illustrates some of the most important valleys of the conduction band.

C. Recombination

In MC simulation of optoelectronic devices, special attention needs to be paid for generation/recombination processes. In our LED simulation, we approximate the recombination rates during the simulation using the density based model given by (see, e.g., Ref. [18] for details)

$$R = \left[\frac{1}{\tau_p(n+n_1) + \tau_n(p+p_1)} + B + C(n+p) \right] \left(np - n_i^2 \right), \quad (1)$$

where τ_n and τ_p are the defect recombination lifetimes for electrons and holes, n and p are the electron and hole densities, n_1 and p_1 are the electron and hole densities when the Fermi level is at the defect state responsible for the defect recombination, B is the net radiative recombination coefficient, C is the Auger recombination coefficient, and n_i is the intrinsic carrier concentration. The terms between square brackets describe the Shockley-Read-Hall (SRH) recombination through defect states, radiative recombination, and Auger recombination, respectively.

The recombination rate given by Eq. (1) is used to remove electrons and holes from the carrier distributions close to the band edges. In the case of Auger recombination, an additional electron (hole) is chosen for each *nnp* (*npp*) event and excited to a state within the conduction (valence) band with its energy increased by the recombination energy. As the recombination processes occur predominantly for carriers close to band edges, also in the MC simulation the Auger-excited electrons and holes are chosen from carriers within a few k_BT from the band edge.

D. Band structure

For the band structures in the MC simulation, we use both the analytic model provided in Ref. [19] based on the full band structure of Ref. [20], as well as analytical band structures fitted to our in-house density functional theory calculations. The density functional calculations use the Heyd-Scuseria-Ernzerhof (HSE) hybrid functional, which has been shown to reproduce band gaps in a good agreement with experimental values [21], [22]. In terms of device-level characteristics, the most important difference between the band structures of Ref.

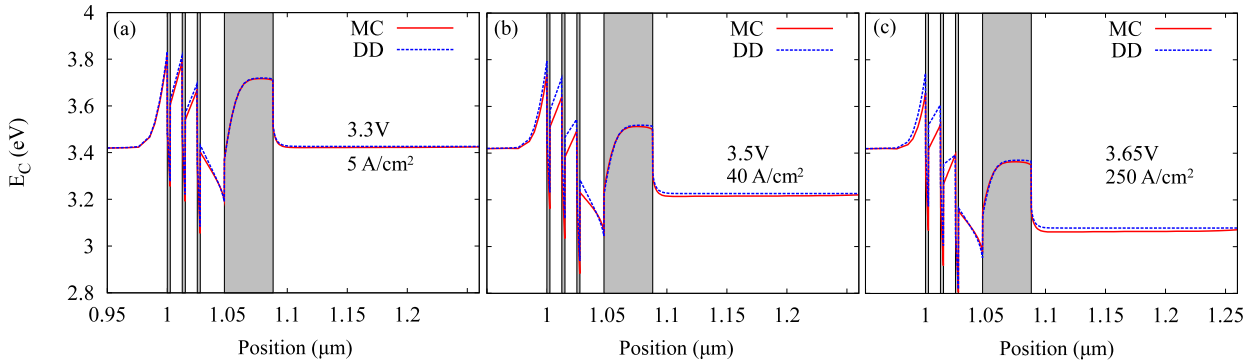

Fig. 4. Conduction band edges from the MC and DD simulations at bias voltages of (a) 3.3 V, (b) 3.5 V, and (c) 3.65 V. The solid curve results from the bipolar MC simulation, and the dashed curve is from the DD simulation. The n-type GaN is on the left, the MQW region and EBL are in the middle, and the p-type GaN is on the right. The EBL is further highlighted with a gray background.

[19] and the detailed density functional theory calculations is expected to be the intervalley separation between the Γ_1 and U valleys. Figure 3 shows the full band structure of GaN calculated using the HSE hybrid functional and also illustrates the most important valleys of the conduction band.

III. Results & Discussion

The bipolar MC model described in Section II is deployed to simulate electron and hole transport in the structures shown schematically in Fig. 1. Material parameters are the same as in Refs. [8], [10]. In the results shown in this section, the band structure is still the one described in Ref. [19].

Figure 4 shows the conduction band edges resulting from the bipolar MC simulation and the plain DD simulation for bias voltages of (a) 3.3, (b) 3.5, and (c) 3.65 V. The current densities are marked in the figures. All the figures are plotted through the MQW region starting from the n-type GaN and ending at the p-type GaN. The EBL is further highlighted with a gray background. Figure 4(a) on the left shows very little difference between the DD and MC results, confirming that DD and MC give similar results in the case where there are no high fields or significant Auger recombination creating hot carriers. Figures 4(b) and (c), on the other hand, exhibit increasing differences between the DD and MC results due to non-quasiequilibrium carrier transport, which is only accounted for in MC. The hot carriers are generated both by Auger recombination and the potential drop over the MQW region. However, the MC result exhibits notably smaller electric fields in the p-type GaN than the previous MCDD model (see the band diagrams in Ref. [8]). This suggests that the hole density of the bipolar MC model is able to screen the hot-electron population better than the frozen hole density of the MCDD.

Figure 5 shows the hole density from the MC and DD simulations at a bias voltage of 3.65 V, for which the current density is already 250 A/cm^2. The curves show that even at such a very high current density, the hole densities from MC and DD show only slight differences in the MQW and EBL. On the contrary, the hole density from MC is more than 10^{19} m^{-3} in the n-type GaN on the left, in contrast with the DD hole density of $\sim 10^{12}$ m^{-3} (note that the electron density is still much larger in that region, namely 10^{24} m^{-3}). The larger hole density of the MC simulation is a direct signature of hot holes

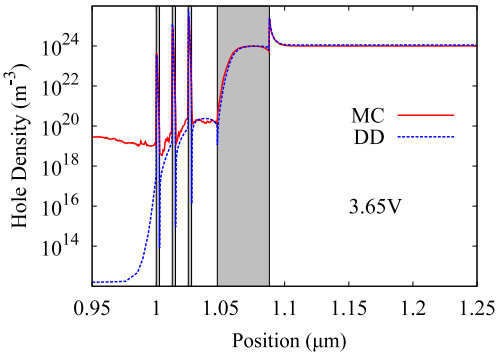

Fig. 5. Hole density from the MC (solid curve) and DD (dashed curve) simulations. The bias voltage is 3.65 V and the current density in MC is 250 A/cm^2.

that are generated in the MQW region and transported towards the n-type contact. This shows that the MQW potential drop and Auger recombination also create a significant population of hot holes. The MC hole density starts to decrease towards the n-type contact further away from the MQW region.

Figure 6(a) shows the current-voltage characteristics and Fig. 6(b) the external quantum efficiency (EQE) resulting from the MC and DD simulations. The bipolar MC simulation predicts slightly higher current densities for a given voltage than DD. The difference is caused by non-quasiequilibrium carrier transport which is not accounted for in DD. In Fig. 6(b), both EQE curves show the efficiency droop starting at a current density slightly below 10 A/cm^2. Result from the MC simulation shows a smaller efficiency due to loss of Auger-generated carriers and carrier overflow. However, the overall contribution of hot carriers to the EQE remains modest in the device chosen for this simulation.

Figure 7 shows the electron density in the U valley of the conduction band throughout the p-type GaN region for different bias voltages. Electron density in the U valley decreases strongly mainly due to intervalley relaxation to the lowest-lying Γ valley. As the U valley is located roughly 1.5 eV over the conduction band minimum in the present band structure model, the whole U valley electron population is created by Auger recombination. Increasing the bias voltage

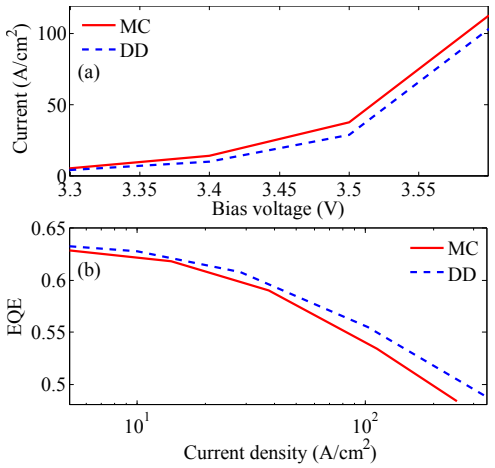

Fig. 6. (a) Current-voltage characteristics and (b) external quantum efficiency as a function of current density from the MC (solid curve) and DD (dashed curve) simulations.

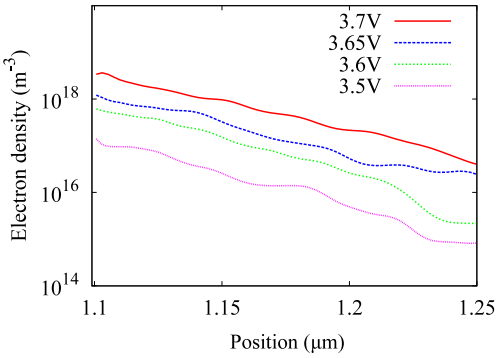

Fig. 7. Electron density in the U valley of the conduction band in the p-type GaN.

also increases the U valley electron density due to increasing the Auger recombination rate.

IV. Conclusions

We carried out bipolar Monte Carlo (MC) simulations of electron and hole transport in a MQW LED device including an electron-blocking layer. The fully bipolar MC simulation resulted in a better convergence than the earlier-generation Monte Carlo–drift-diffusion model and also provided indications of hot holes. Accounting for non-quasiequilibrium transport of both electrons and holes increased the current and decreased the efficiency especially at high currents. Coupling our in-house full band structure calculations to the MC simulation will enable even more detailed predictions of the full device operation.

Acknowledgment

We acknowledge the Aalto Energy Efficiency Programme (AEF), the Academy of Finland, and the Nokia Foundation for support.

References

[1] S. Nakamura and M. R. Krames, "History of Gallium-Nitride-Based Light-Emitting Diodes for Illumination," *Proc. IEEE*, vol. 101, pp. 2211–2220, 2013.

[2] J. Piprek, "LED droop: A critical review and novel solution," *Compound Semiconductor*, vol. 20, pp. 44–48, 2014.

[3] J. Piprek, F. Römer, and B. Witzigmann, "On the uncertainty of the Auger recombination coefficient extracted from InGaN/GaN light-emitting diode efficiency droop measurements," *Appl. Phys. Lett.*, vol. 106, pp. 101101, 2015.

[4] P. Kivisaari, J. Oksanen, and J. Tulkki, "Polarization doping and the efficiency of III-nitride optoelectronic devices," *Appl. Phys. Lett.*, vol. 103, pp. 211118, 2013.

[5] J. Iveland, M. Piccardo, L. Martinelli, J. Peretti, J. W. Choi, N. Young, S. Nakamura, J. S. Speck, and C. Weisbuch, "Origin of electrons emitted into vacuum from InGaN light emitting diodes," *Appl. Phys. Lett.*, vol. 105, pp. 052103, 2014.

[6] M. Binder, A. Nirschl, R. Zeisel, T. Hager, H.-J. Lugauer, M. Sabathil, D. Bougeard, J. Wagner, and B. Galler, "Identification of *nnp* and *npp* Auger recombination as significant contributor to the efficiency droop in (GaIn)N quantum wells by visualization of hot carriers in photoluminescence," *Appl. Phys. Lett.*, vol. 103, pp. 071108, 2013.

[7] T. Sadi, P. Kivisaari, J. Oksanen, and J. Tulkki, "On the correlation of the Auger generated hot electron emission and efficiency droop in III-N light-emitting diodes," *Appl. Phys. Lett.*, vol. 105, pp. 091106, 2014.

[8] T. Sadi, P. Kivisaari, J. Oksanen, and J. Tulkki, "Microscopic simulation of hot electron transport in III-N light-emitting diodes," *Opt. Quant. Electron.*, vol. 47, no. 6, pp. 1509–1518, 2015.

[9] P. Kivisaari, J. Oksanen, J. Tulkki, and T. Sadi, "Monte Carlo simulation of hot carrier transport in III-N LEDs," *J. Comput. Electron.*, vol. 14, no. 2, pp. 382-397, 2015.

[10] P. Kivisaari, T. Sadi, J. Oksanen, and J. Tulkki, "Bipolar Monte Carlo simulation of electrons and holes in III-N LEDs," *Proc. SPIE*, vol. 9363, pp. 93631S, 2015.

[11] C. Jacoboni and P. Lugli, *The Monte Carlo Method for Semiconductor Device Simulation*, Springer-Verlag, Wien, 1989.

[12] T. Sadi, R. W. Kelsall, and N. J. Pilgrim, "Investigation of self-heating effects in submicrometer GaN/AlGaN HEMTs using an electrothermal Monte Carlo method," *IEEE. Trans. Electr. Dev.*, vol. 53, pp. 2892–2900, 2006.

[13] T. Sadi and R. W. Kelsall, "Hot-phonon effect on the electrothermal behavior of submicrometer III-V HEMTs," *IEEE Electr. Dev. Lett.*, vol. 28, pp. 787–789, 2007.

[14] T. Sadi and R. W. Kelsall, "Theoretical study of electron confinement in submicrometer GaN HFETs using a thermally self-consistent Monte Carlo method," *IEEE Trans. Electr. Dev.*, vol. 55, pp. 945–953, 2008.

[15] T. Sadi, R. W. Kelsall, N. J. Pilgrim, J.-L. Thobel, and F. Dessenne, "Monte Carlo study of self-heating in nanoscale devices," *J. Comput. Electron.*, vol. 11, pp. 118–128, 2012.

[16] C. Jacoboni and L. Reggiani, "The Monte Carlo method for the solution of charge transport in semiconductors with applications to covalent materials," *Rev. Mod. Phys.*, vol. 55, pp. 645–705, 1983.

[17] B. K. Ridley, *Quantum Processes in Semiconductors*, Clarendon Press, Oxford, 1999.

[18] O. Heikkilä, J. Oksanen, and J. Tulkki, "Ultimate limit and temperature dependency of light-emitting diode efficiency," *J. Appl. Phys.*, vol. 105, pp. 093119, 2009.

[19] J. D. Albrecht, R. P. Wang, P. P. Ruden, M. Farahmand, and K. F. Brennan, "Electron transport characteristics of GaN for high temperature device modeling," *J. Appl. Phys.*, vol. 83, pp. 4777, 1998.

[20] R. Wang, P. P. Ruden, J. Kolnik, I. Oguzman, and K. F. Brennan, "Dielectric Properties of Wurtzite and Zincblende Structure Gallium Nitride," *J. Phys. Chem. Solids*, vol. 58, pp. 913–918, 1997.

[21] Q. Yan, P. Rinke, M. Scheffler, and C. G. Van de Walle, "Strain effects in group-III nitrides: Deformation potentials for AlN, GaN, and InN," *Appl. Phys. Lett.*, vol. 95, pp. 121111, 2009.

[22] Q. Yan, P. Rinke, A. Janotti, M. Scheffler, and C. G. Van de Walle, "Effects of strain on the band structure of group-III nitrides," *Phys. Rev. B*, vol. 90. 125118, 2014.